ORIGINAL ARTICLE

Geometry simplification of open-cell porous materials for elastic deformation FEA

Camilo Cortés[1] · Maria Osorno[2] · David Uribe[2] · Holger Steeb[2] · Oscar Ruiz-Salguero[3] · Iñigo Barandiarán[4] · Julián Flórez[1]

Abstract
Estimation of mechanical properties of porous materials is central for their medical and industrial application. However, the massive size of accurate boundary representations (B-Rep) of the foams makes the numerical estimations intractable. Even for small domain sizes, the mesh generation for finite element analysis (FEA) may not terminate. Current efforts for simulating porous materials use statistical predictions of the material structure. The simulated and actual materials present different geometry and topology, with consequences on the simulation results. To overcome these limitations, this manuscript presents a method, which (1) synthesizes an accurate truss abstraction from the raw geometry data, (2) executes efficient FEA simulations, and (3) processes nodal displacements to estimate apparent mechanical moduli of the porous material. The method addresses materials whose ligaments have circular cross-sections. The iso-surface present in the Computer Tomography (CT) scan of the porous material is used to synthesize a truss graph whose edges are truncated cones. Then, optimization and simplification methods are applied to produce a topologically and geometrically correct truss representation for the foam domain. Comparative FEA load simulations are conducted between the full B-Rep and truss representations of the material. The truss model proves to be significantly more efficient for FEA, departing from the Full B-Rep FEA by a maximum of 16% in the estimation of equivalent mechanical moduli. Geometric assessments such as porosity and Hausdorff distance confirm that the truss abstraction is a cost-effective one. Ongoing efforts concentrate on point set geometric algorithms for enforcement of standardized material testing.

Keywords Geometry simplification · Open-cell foams · Elastic properties · FEA

✉ Camilo Cortés
ccortes@vicomtech.org

Maria Osorno
maria.osorno@mechbau.uni-stuttgart.de

David Uribe
david.uribe@mechbau.uni-stuttgart.de

Holger Steeb
holger.steeb@mechbau.uni-stuttgart.de

Oscar Ruiz-Salguero
oruiz@eafit.edu.co

Iñigo Barandiarán
ibarandiaran@vicomtech.org

Julián Flórez
jflorez@vicomtech.org

1 eHealth and Biomedical Applications Department, Vicomtech, Mikeletegi Pasealekua 57, Donostia-San Sebastián, Spain

2 Institute of Applied Mechanics, University of Stuttgart, Pfaffenwaldring 7, Stuttgart, Germany

3 Laboratorio de CAD CAM CAE, Universidad EAFIT, Carrera 49 No. 7 sur 50, Medellín, Colombia

4 Industry and Advanced Manufacturing Department, Vicomtech, Mikeletegi Pasealekua 71, Donostia-San Sebastián, Spain

Glossary

BB	Bounding box
B-Rep	Boundary representation of a solid in R^3. The usual topological hierarchy: BODY (3D), LUMP (3D), SHELL (2D), FACE (2D), LOOP (1D), EDGE (1D), VERTEX (0D). FACEs (i.e. 'trimmed surfaces') may be mounted on either smooth surfaces or planes (triangles)
CT	Computer tomography
FE	Finite element
FEA	Finite element analysis
FEM	Finite element method
MCF	Mean curvature flow
Reference model	Model to measure the simplification against. In this manuscript the Reference model is the Full B-Rep of the foam
ϵ_k	Strain in k direction
$E(\epsilon)_k$	Apparent Young Modulus at strain ϵ caused by loads in k direction
$G(\epsilon)_k$	Apparent Shear Modulus at strain ϵ caused by loads in k direction
$V(\epsilon)_{ij}$	Apparent Poisson ratio computed from a contraction in j direction given an extension in i direction
ϕ	Porosity of a porous material sample

1 Introduction

Foam materials present remarkable mechanical, thermal, electrical and acoustic properties, which make them ideal for many aerospace, industrial and medical applications [1–4]. However, precisely these property differences represent uncertainties for object design processes. Foam materials present open-cell or closed-cell structures. The open-cell structure (Fig. 1a) is formed by a set of connected ligaments located at the edges of random polyhedral cells [4–6]. The closed-cell structure (Fig. 1b) consists of the set of connected facets located at the faces of random polyhedral cells [7, 8]. In open-cell porous materials, the pore space is connected across the full domain. In closed cell materials, the porous space of each cell is enclosed by the cell walls. This article addresses open cell porous materials.

For the numerical simulation of cellular solids, it is important to generate digital representations of the porous materials that: (1) accurately model the material topology and geometry and (2) are computationally efficient. However, the complex geometry of the porous material makes computationally intensive to achieve an useful digital model.

To reduce the computational expenses of mechanical simulations using a full 3D representation of open-cell foams, this investigation uses a simplified geometry. This manuscript presents a workflow to obtain the reduced representation of the open-cell foam and the assessment of the geometrical and mechanical effectiveness of the simplified model.

2 Literature review

The generation of geometric models of foam microstructure and properties can be classified into models (1) of actual samples and (2) statistically generated.

1. Actual sample models: these models mimic a specific sample (e.g. CT [9–13]). This approach guarantees high fidelity to the original foam geometry and topology. However its application is limited by: (a) the heavy and time consuming manual work required to make the model suitable for FEA meshing (with 3D elements), (b) the unaffordable memory and time computer expenses

Fig. 1 Porous material structures: **a** open cell, **b** closed cell

(a)   **(b)**
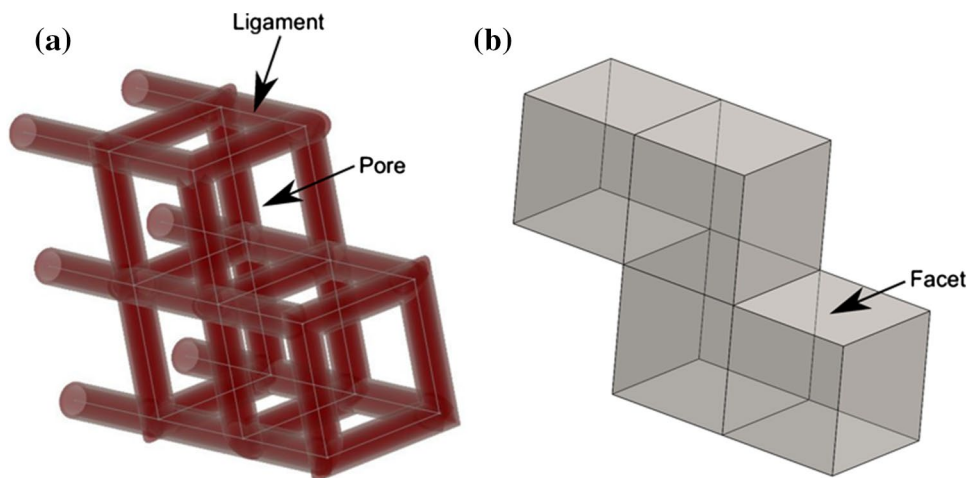
[3, 9, 11], and (c) the small (non-representative) volumes that can be simulated [4].

2. Statistically generated models: these models do not reconstruct the actual geometry and topology of a foam sample. Instead, they aim to represent its geometry in a stochastic sense.

   (a) Arrays of identical (unit) cells: a popular one is the Kelvin Cell (tetrakaidecahedron [4, 6, 14–16]). Anisotropic and perturbed versions of the Kelvin cells have been proposed to better fit the geometry of real foams. The advantage of the Unit-Cell method is that the bulk behavior of the foam can be estimated from a single cell or a small cluster of cells (representative volume). However, this method does not grasp: (a) the large variation in the cell size and shape [5] and (b) the presence of manufacturing defects in real foams [3].

   (b) Tessellations: These approaches generate space partitions Voronoi [3, 16] and Laguerre [5, 17–19] from which foam-like structures are generated. Tessellations approximate better the irregular cell shape of actual foams. Some tessellation approaches are able to model foam defects [3] such as closed windows, small windows, and missing ligaments in cells. Tessellation-based foam models require 3D FEA meshing to be used, which represents a serious disadvantage.

As reviewed, the existing approaches are impractical (in case of Finite 3D Element Analysis), or else, generate virtual domains based on statistical properties of foams. In contrast, this article presents a method that produces a simplified CT-based model for efficient FEA simulation. The simplified model aims to overcome the difficulties imposed by the computational expenses of simulating a full 3D model, while reasonably preserving the geometry and topology of the original sample. In the present investigation, the ligaments of the porous material are modeled as beams of circular cross-section with variable diameter fully constrained in the nodes or junctions with other ligaments. The algorithm applies to foams with ligaments having approximately circular cross-sections (Fig. 2). This simplified representation presents high fidelity to the original geometry and topology of the foam specimen of interest, preserving its specific features and natural imperfections. Because the simplified geometrical model uses 1D beams instead of 3D tetrahedra of the full B-Rep representation, the implemented approach presents advantages in estimating apparent mechanical moduli of porous materials.

This method pragmatically articulates well-known simple and complex algorithms of computational geometry. The simplification produces a significant reduction in the
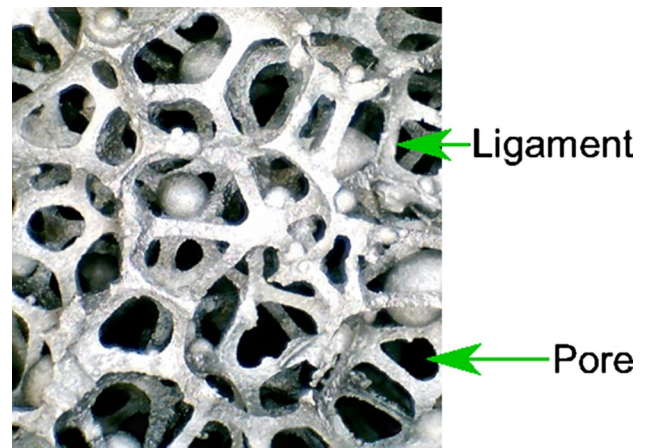

Fig. 2 Porous material whose ligaments have approximately circular cross-sections

computing resources consumed by mechanical simulations of porous materials.

2.1 Contributions of this article

This manuscript presents: (a) a methodology to produce a simplified model for efficient FEA simulation of open-cell porous materials and (b) the evaluation of the simplified model from the geometric and mechanical viewpoints. This manuscript presents the following aspects, needed to make the geometry simplification useful for engineering applications:

1. Simplified modeling of foam: accurate approximation of foam ligaments with 1D FEA elements (beam), which are much more efficient in computer resources than 3D solid (i.e. Full B-Rep) models.
2. Geometry assessment of the simplified model: estimation and comparison of the porosity coefficient (up to 0.17% error) and Hausdorff Distance (up to 0.2% error) with respect to a Full B-rep model.
3. Mechanic assessment of the simplified model: estimation and comparison of equivalent mechanical moduli (Apparent Young, Shear, and Poisson) of the simplified model with respect to a Full B-rep model (up to 16% error).

3 Materials and methods

The simplified geometry (truss data) presents clear advantages for FEA with respect to the full B-Rep model. Figure 3 shows a comparison of the processes to produce B-Rep vs. Truss input for an FEA. The process starts with the CT scan of the domain $\Omega \subset R^3$, which is basically a scalar field CT:
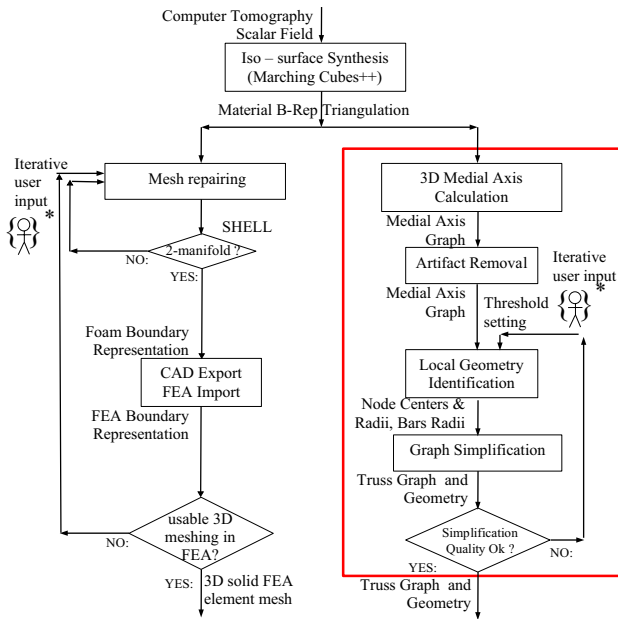
Fig. 3 Comparison between full B-Rep and truss formats pre-processing. *: iterative human interaction

$\Omega \to R$. An iso-surface in triangular format is extracted from Ω (using Marching Cubes [20] or any other iso-surface synthesis algorithm). The left branch produces a full B-Rep (i.e. 3D solid model) of the porous domain. The right branch produces a truss (nodes + bars) representation of the porous domain.

1. *B-Rep foam domain data* The left branch (Fig. 3) is a well-known user-assisted approach, in which most of the user effort is invested in repairing the triangular mesh. It is necessary to solve conflicts such as: holes, non-manifold edges, intersecting faces, degenerate faces, spikes, excessive number of triangles, among others. Most of these conflicts can be solved automatically by using advanced software like Geomagic, Rhinoceros 3D, etc. However, there are cases in which mesh reparing conflics appear and manual intervention is necessary to defeature problematic zones of the triangular mesh. In the application that we address in this work, those conflicts are prone to appear, since noise and artifacts are generated by the CT scan and reconstruction process of the complex geometry of the metallic foam. Mesh repairing operations must be repeated if the FEA module rejects the B-Rep achieved. If the FEA module accepts the B-Rep, the 3D meshing typically takes a significant amount of time and may even surpass hardware memory capability.

2. *Truss domain data* The right branch (Fig. 3) process takes a triangular B-Rep and produces a truss (nodes + bars) model of the porous material, as follows: (a) a

Medial axis skeleton of the triangular B-Rep is calculated. (b) Artifacts and "hairs" are removed from the skeleton. (c) Center and radius of nodes and truncated cone parameters for the bars are estimated. (d) Node merging or node insertion (as needed) are conducted, to ensure topologic and geometric correctness of the output truss representation. The manual adjustment of parameters of the simplification method related to sampling and minimum feature preservation may be needed (details are given in the following sections). Simplification quality is assessed in terms of porosity and Hausdorff distance, as discussed in Sect. 4.2. After the truss model is obtained, 3D meshing for FEA is not required because truss struts can be directly represented with 1-D beam elements in the FEA software. In this way, the high computational costs and user interaction that 3D meshing requires is avoided with this methodology.

The following sections describe in detail the process to calculate the truss-based simplified geometry.

3.1 Open-cell foam geometry simplification problem

Given A surface triangular mesh (Fig. 4a) obtained from CT scan voxel-based data of a foam specimen (details of the voxel-to-triangular mesh conversion in [21]). The surface triangular mesh satisfies being manifold and watertight.

Goal To generate a graph (nodes and edges) representation of the foam model in which:

(a) Each foam ligament is approximated with a strut element of varying cross-section (Fig. 4b). Highly curved ligaments are represented with several struts. The truss abstraction consists of using 1-D elements (truncated cone bars) which meet in the graph nodes. Notice that their graphic representation would seem to include self-intersections at the nodes. However, this is only a graphical representation of the graph structure and does not correspond to a well-formed surface.

(b) Each node and bar of the simplified model has the actual sizes of the corresponding spot in the foam. Therefore, the topology and geometry of the foam are approximated with high fidelity.

3.2 Simplification to Truss model

The implemented algorithm includes the generation of an undirected graph $G(E, V, R)$ (Fig. 5), which represents the truss model of the foam. E is the set of edges, V is the set of nodes and R is the set of radii associated with the edges E. The edges of G approximate straight ligaments of the foam. Curved ligaments require several edges. The nodes V

Fig. 4 Input and output of the simplification method. **a** Foam triangular boundary representation. **b** Graphical abstraction of foam truss representation (abstraction does not have to be manifold)
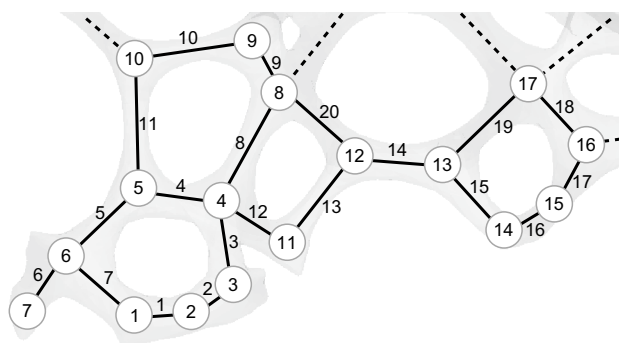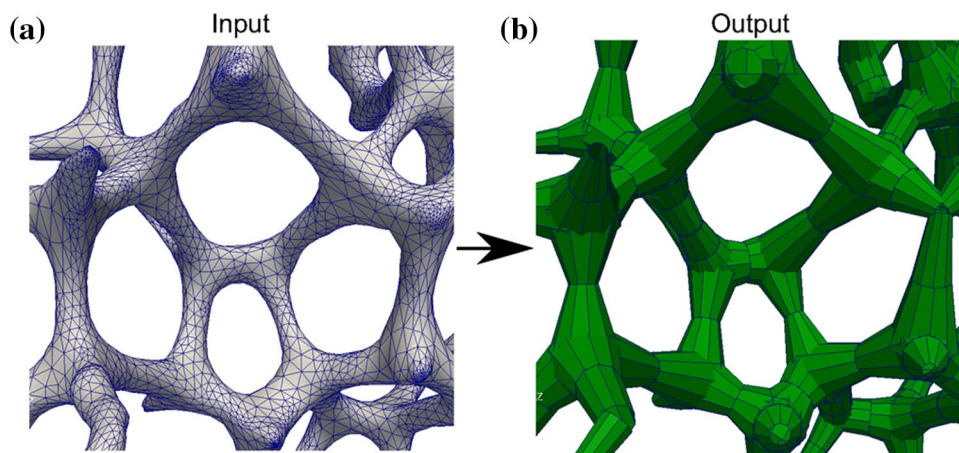
Fig. 5 Undirected Graph $G(E, V, R)$ to generate the truss representation of the foam

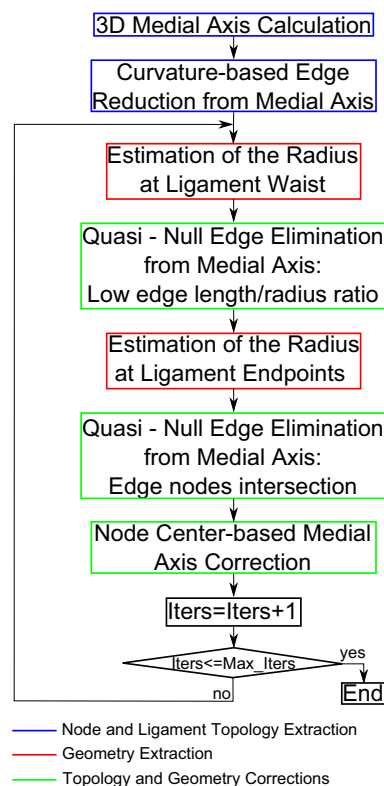**Fig. 6** Workflow of the truss model generation

correspond to the endpoints of the ligaments. The struts are represented as truncated cones, whose parameters are the initial and final vertices, and the initial and final radius. The set of radii is stored in R.

Figure 6 shows the order and priority in which the steps of the method to generate the truss model are applied. Please notice that the mentioned steps are classified into three categories: (1) node and ligament topology extraction, (2) geometry extraction and (3) topology and geometry corrections, which are discussed in detail in the following sections.

An iterative process prunes the graph $G(E, V, R)$, eliminating degenerate quasi-null edges. Although in each iteration the obtained model can be used for FEA, more iterations mean a higher level of simplification. The iterations are automated, using as input a rough estimation of pore ligament diameter and length, which is usually available. A discussion of the used methodology follows.

3.2.1 Node and ligament topology extraction

The objective of this step is to obtain the set of edges E and nodes V of the graph $G(E, V, R)$. An initial skeletal (medial

axis) representation of the foam is generated, which is later simplified to produce the truss representation of the foam.

Medial axis estimation The medial axis of the foam (Fig. 7) is estimated using Mean Curvature Skeletons ([22]). This method uses the Mean Curvature Flow (MCF) to iteratively collapse the 3D foam domain (represented by a triangular mesh) into a medially piecewise linear centered curve. This method preserves the topology of 3D domains, which is a key feature for foam simplification. In this work, the method in [22] is used because of its successful performance

Fig. 7 Medial axis estimation of the foam. **a** Input mesh; **b** iteration 1 of the MCF-based method [22]; **c** iteration 15 of the MCF-based method; **d** the estimated medial axis vs. input mesh

(a) **(b)** **(c)**

(d)
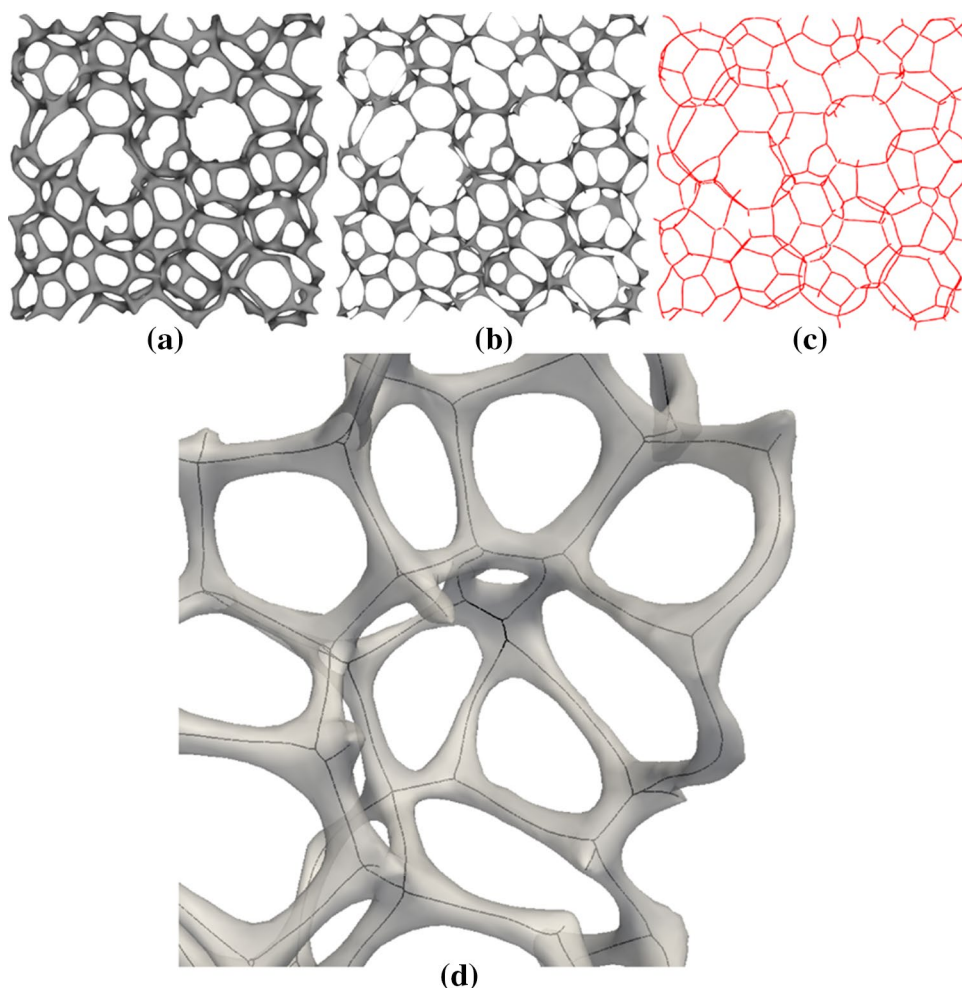
assessments reported in [23, 24] and the availability of its source code [25], but any other similar method can be used.

Curvature-based Edge Reduction from Medial Axis. The medial axis graph $G(E, V, R)$ contains artifacts and is over-lycrowded. The next step is to represent such a graph using a reduced set of straight segments. Sequences of edges whose nodes have degree ≥ 2 are replaced by sequences of longer edges (Fig. 8a). The number of edges to be used in the simplified path T_s is controlled by a recursive algorithm that checks the maximum distance between the original path, T_0, and T_s. If the maximum distance is larger than a configurable threshold D_t, a new edge is added to T_s and the vertices of T_s are re-arranged to reduce the maximum distance between T_0 and T_s. Figure 8b illustrates the simplification of paths T_0. Figure 8c shows the result of the curvature-based medial axis simplification.

3.2.2 Preliminary geometry extraction

The objective of this step is to obtain the set R by approximating the radius of the ligaments that surround edges E at the vertices and center of the edges. Based on the results of

such estimations, additional corrections on $G(E, V, R)$ are performed.

Estimation of the radius at ligament waist Consider a ligament edge $e_k = (v_i, v_j)$ with associated point set as in Fig. 9a. At the middle of edge e_k, a half space is defined as the thin infinite space contained between two close parallel planes Π_1 and Π_2, which are perpendicular to edge e_k. This thin infinite slab contains a nearly cylindrical point subset of the ligament point set. Distance D_e is user defined and determines the search radius of points that belong to the foam triangular mesh that will be used to build the cylindrical point subset. Figure 9a presents the radius of this cylinder. This radius is easily approximated (along other methods) by the average distance of the cylinder points to the axis e_k. Figure 9b draws a neighborhood of the foam, with cylinders having the estimated radii as a first approximation of the ligaments. Notice that an edge e_k engenders two truncated cone beams, with r as their radius at the waist (approx. midpoint of e_k).

Estimation of the radius at the ligament endpoints For a node $v_i \in V$ with degree ≤ 2, the method to estimate the radius of a ligament at v_i is similar to the one described

Fig. 8 Medial axis simplification. **a** Simplification of graph paths bounded by nodes with degree > 2; **b** examples of the simplification of graph paths; **c** result of the curvature-based medial axis simplification
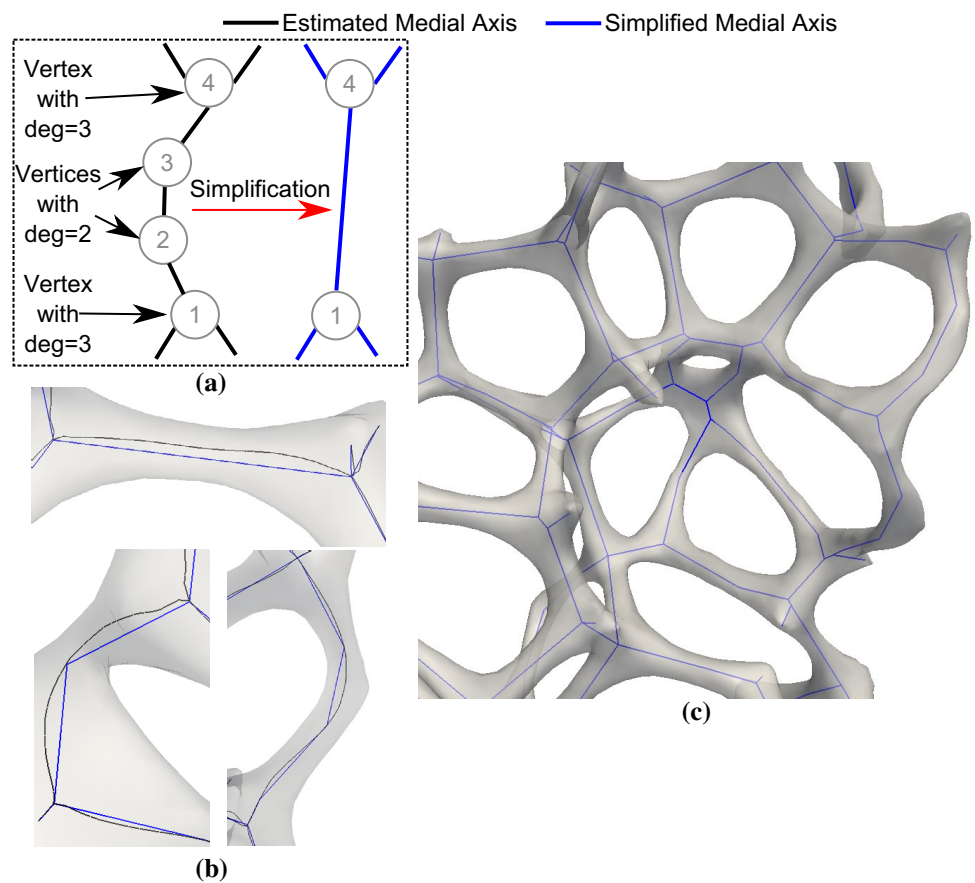
Fig. 9 **a** Estimation of the ligament radius at the midpoint of edge e_k; **b** result of the ligament radius estimation at midpoints of edges E
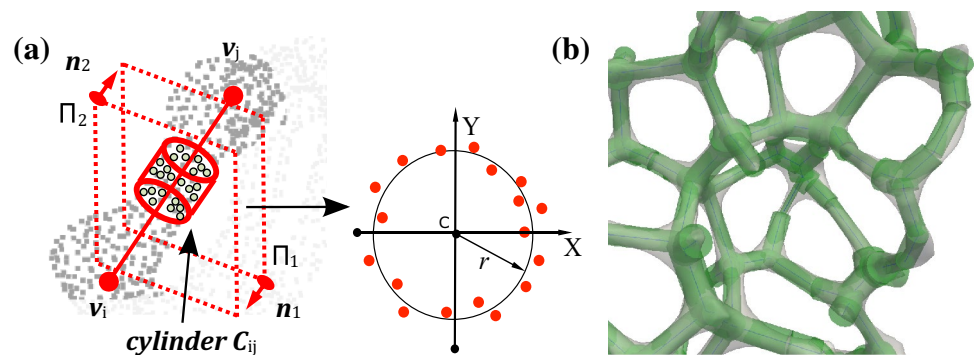

in 3.2.2. For nodes v_i with degree > 2 (Fig. 10a), r is estimated as the radius of the sphere fitted to points on the foam mesh within an user-defined search radius D_n ($D_n > D_e$) with normal **n** approximately aligned with vector $\mathbf{v} = (P_s - P_v)/\lVert P_s - P_v \rVert$.

In Fig. 10, each node v_i is represented by a sphere with the estimated radius r. Figure 10b shows the results of the estimation of the ligament radius r at the nodes V for a region of the foam.

A double-criterion method (distance + direction of normals) is used to estimate the ligament waist and node radius because they provide more robustness compared to pure distance-based methods. Consider the case in which reconstruction artifacts cause the B-Rep model to present internal cavities (Fig. 11). In such case, the double-criterion method filters out the points based on the normal direction. Green points are filtered out and only orange points are used in the radius estimation. On the contrary, a distance-based method would consider green and orange points, under or overestimating the ligament waist or node radius. The double-criterion method is not faultless but provides an additional robustness condition compared to pure distance-based

Fig. 10 **a** Ligament radius estimation at node v_i with degree > 2; **b** result of the estimation of the radius of the ligaments at nodes V
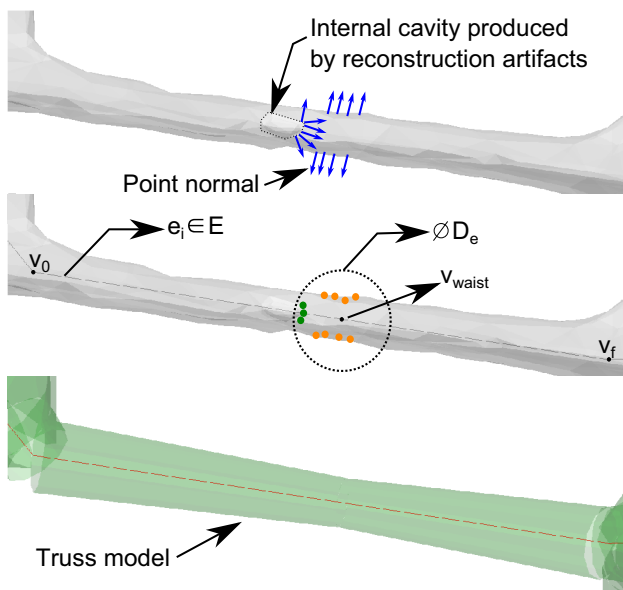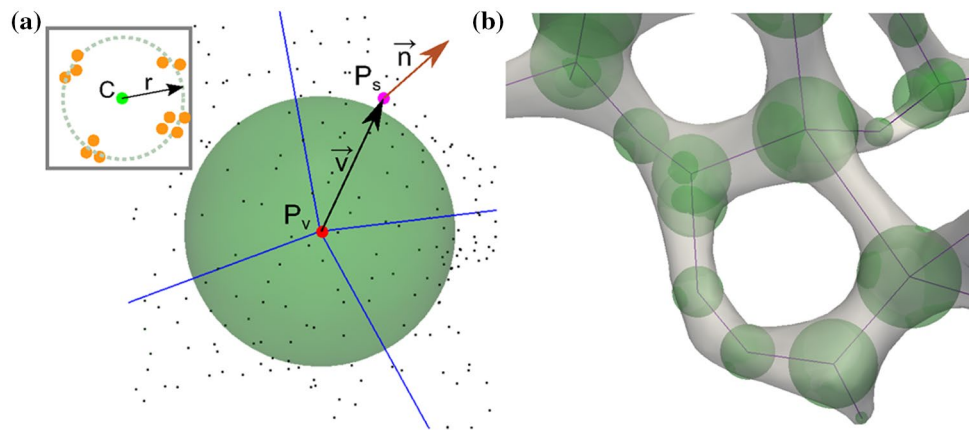
Fig. 11 Filtering of points using the double-criterion method for estimation of edge/node radius

methods. The mentioned artifacts are common in foam scans and are difficult to detect and manually eliminate when producing a Full B-Rep model from the CT scan data.

Please note that D_e and D_n have a direct physical meaning, which is the expected ligament waist radius and node radius, respectively. Reasonable initial guesses for D_e and D_n can be obtained from foam technical specifications or from CAD software. The values of D_e and D_n used in the experiments presented in this article are reported in Sect. 4.

3.2.3 Topology and geometry corrections

Based on the estimations performed in previous sections, optimization and corrections can be performed on the E and V sets of $G(E, V, R)$.

Quasi-null edge elimination from medial axis To avoid having an excessive amount of struts in the approximation of ligament junction regions of the foam, two strategies have been implemented to detect and collapse dispensable edges in $G(E, V, R)$:

1. Low edge length/radius ratio. This strategy assesses if a very short edge is being used to approximate a region of the foam where ligaments are thick (Fig. 12a). If the ratio $l_e/r_e < 1$, where l_e is the length of edge e_i and r_e is the radius associated with the midpoint of e_i, edge e_i is a candidate to be collapsed. An additional condition to collapse e_i is that $l_e < L_s$. L_s is the desired minimum length of the struts that are used to approximate the foam ligaments. This ensures a minimum feature preservation.

   In the collapsing of e_i, its nodes a and b are replaced by a single node c. The coordinates of c are computed as the weighted average of the coordinates of a and b, where the weights are assigned according to the degree of nodes a and b. Figure 12b shows the result of the collapsing of an edge using the length/radius ratio approach.

2. Edge nodes intersection. This strategy assesses if the nodes of an edge are too close to each other based on the estimated ligament radius at the nodes (a very similar strategy for the simplification of the medial axis is used in [26]). If the spheres associated with nodes a and b (Sect. 3.2.2) of edge e_i intersect each other, edge e_i is a candidate to be collapsed (Fig. 13a). Additional conditions to collapse e_i are:
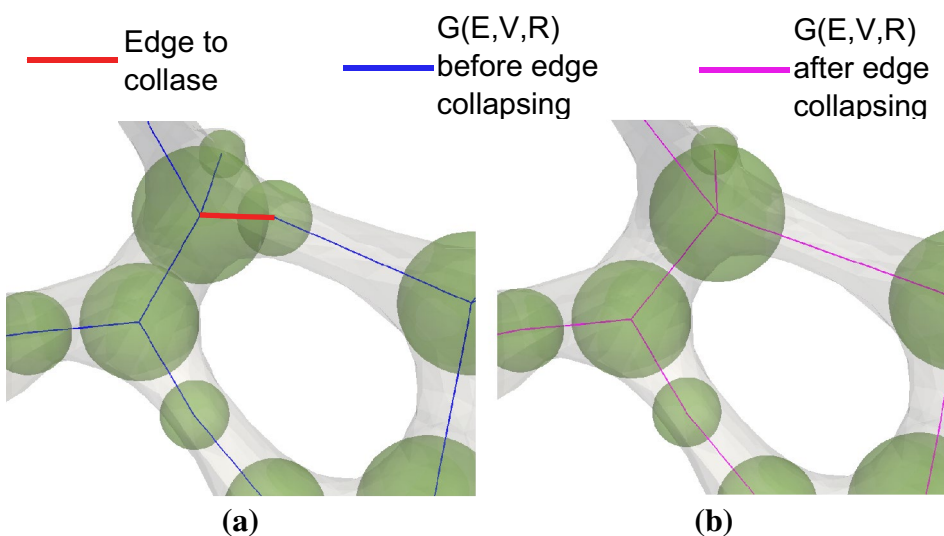
   (a) the length of $e_i < L_l$, where $L_l = 2.5 * L_s$.
   (b) at least one of its nodes presents degree ≤ 2. This avoids the oversimplification of regions of the foam with complex ligament interconnection.

Fig. 12 Edge collapse based on the length/radius ratio criterion

Edge to collase | G(E,V,R) before edge collapsing | G(E,V,R) after edge collapsing

(a) **(b)**
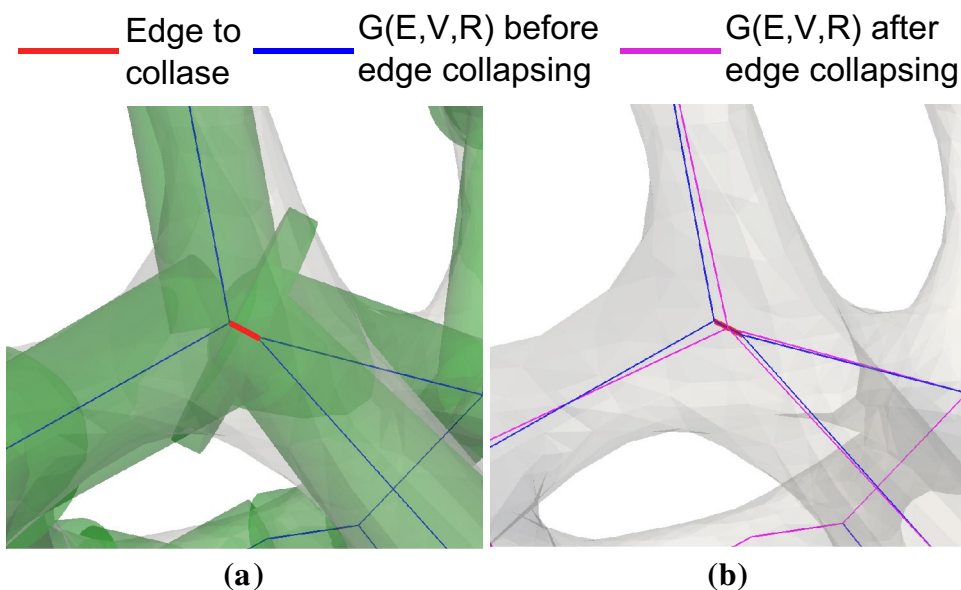
Fig. 13 Edge collapse by the node intersection criterion

Edge to collase | G(E,V,R) before edge collapsing | G(E,V,R) after edge collapsing

(a) **(b)**

The edge collapsing approach is the same used for edges with low length/radius ratio. Figure 13b shows the result of the collapsing of edges using the node intersection-based strategy.

Node center-based medial axis correction Edge collapsing operations can be performed iteratively in order to achieve further simplification of $G(E, V, R)$. However, this may cause significant deviations of the paths of G from the actual medial axis of the foam model. This makes necessary to center the nodes of G with respect to the surrounding surface. To do so, the node is moved towards the center of the sphere obtained in the estimation of the radius of

the ligament at the node (Sect. 3.2.2). The result of this correction on the region in Fig. 13b is shown in Fig. 14.

3.2.4 Synthesis of Truss from graph model

Once $G(E, V, R)$ is corrected, the truss is generated as follows:

1. Split edge e_i at waist v_{waist} into two edges $e_a = (v_0, v_{waist})$ and $e_b = (v_{waist}, v_f)$.
2. Create a new truss vertex at v_{waist}.
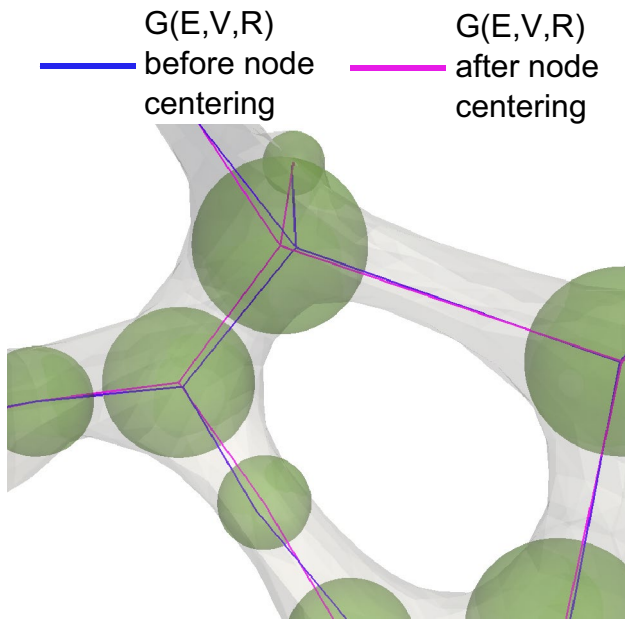3. Identify the strut radii (r_0, r_{waist}, r_f) at endpoints of edges e_a and e_b.

Fig. 14 Node center correction

4. Define tapered cone $C_a = [v_0, r_0, v_{waist}, r_{waist}]$.
5. Define tapered cone $C_b = [v_{waist}, r_{waist}, v_f, r_f]$.
6. Repeat steps 1 to 5 for each $e_i \in E$.

Figure 15 depicts the generation of the truss model from $G(E, V, R)$. Notice that the Truss nodes present multiple incoming bars. For structural simulation, the fact that the incoming idealized bars would overlap each other at the nodes has no effect since the truss model does not come to indeed mesh this abstract geometry. On the other hand, for estimating the truss model porosity (ratio of empty to total volume), such an overlap of beams at the nodes would introduce an error in the account of solid material. To avoid this error in the case of porosity computing, these steps are taken: (a) a sphere is synthesized at the node, whose radius is computed as explained in Sect. 3.2.2, (b) the incoming beams are interpreted as having their length shortened by the amount of the node sphere radius (Fig. 15). The volume of the truss model is estimated adding the volumes of the spheres and shorted beams. In this manner, the wrong repeated account of the overlapping volumes is avoided. The resulting porosity computation shows an agreement of 98.3% with respect to the B-Rep-based porosity calculation.

3.3 Finite element analyses on open-cell foam models

To assess the performance of the truss model for mechanical simulations, the estimation of its elastic properties (apparent Young's Modulus, Poisson's Ratio and Shear
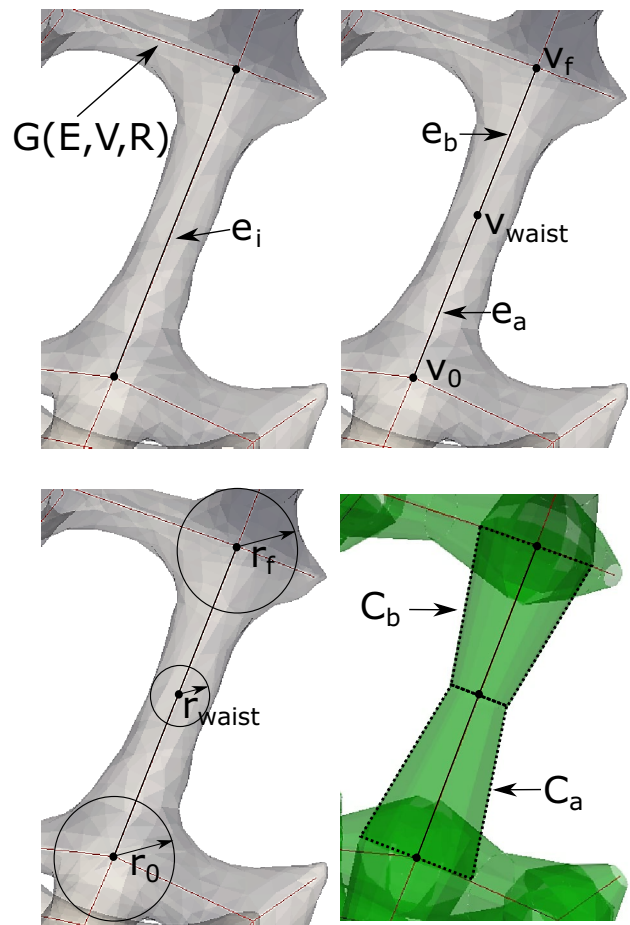
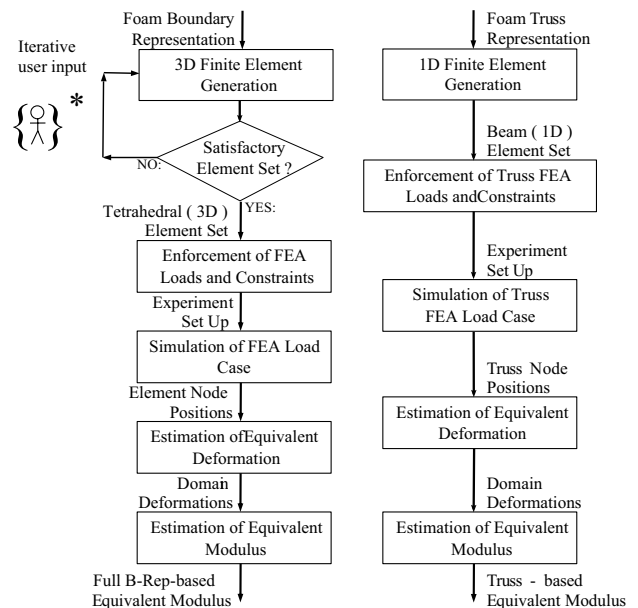**Fig. 15** Generation of the truss model from $G(E, V, R)$

Fig. 16 Comparison between FEA load cases using B-Rep vs. truss porous domain models. *: iterative human interaction

Table 1 Comparative table. Finite Element models Full B-Rep vs. truss for estimation of equivalent moduli of porous materials

Model	Input model	FE mesh	Apparent estimated moduli
Full B-Rep (Reference)	Watertight, manifold, smoothed triangular mesh	Tetrahedral (solid 185)	Young Poisson Shear
Truss	Synthesized graph model (bars and nodes)	Constrained beams (solid 188)	

Modulus) is conducted and compared with the ones of a model of reference (full B-Rep with same domain size). Fig. 16 compares the load FEA cases using full B-Rep (left workflow) vs. truss (right workflow) models of the porous domain. Table 1 summarizes the features of the compared FE models. 3D FEA derived from C^2 (smooth) or C^0 (triangular) full B-Reps is an approach already tried by investigators. 3D FEA is used here to contrast against the faster 1-D FEA derived from truss representations. The emphasis of this manuscript is on the simpler/faster Truss representation and on the explicit calculation of macro-deformations from the set of individual displacements of the truss nodes.

3.3.1 Truss model

The truss model is built in ANSYS by implementing Matlab functions that read $G(E, V, R)$ and produce ANSYS scripts with the corresponding beam elements. ANSYS automatically performs further division of the beam elements based on the length of the beam originally specified in the script.

3.3.2 Reference model

The reference model is obtained by meshing in ANSYS with tetrahedral elements a surface model of the foam extracted from a CT scan. Meshing parameters in ANSYS are manually adjusted to avoid the generation of very small or flat tetrahedra. The obtained mesh is exported in MSH format and Matlab code is written to read the mesh boundary representation.

3.3.3 Mechanical simulations

Tension (Fig. 17) and shear (Fig. 18) case studies are generated in ANSYS to estimate the elastic properties of the reference and truss models. Each case study setup is defined using ANSYS scripts generated from custom Matlab functions. This process allows to control that:

1. the number, direction and magnitude of applied displacement constraints and loads is the same for both models.
2. the 3D position of constrained/loaded nodes is the closest between the models.

The summary of the setup of the mechanical simulations is presented in Table 2. The applied stress is chosen to assess the models in their linear elasticity region, in agreement with the experimental data in [27–29] for open-cell foams with 5–6% relative density.
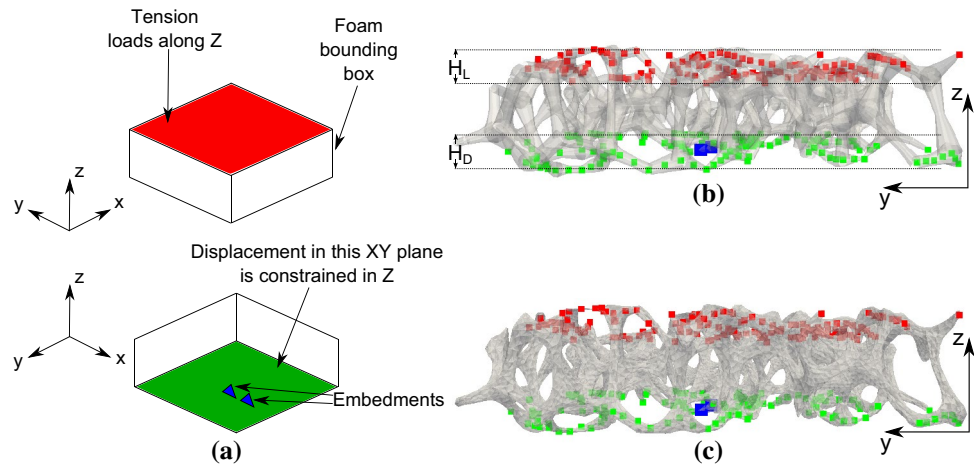
Tension case study The setup of this case study is shown in Fig. 17. Displacement constraints are applied on the nodes on the lower *X–Y* plane of the foam BB. For nodes in green, the displacements along *Z* are set to zero. For nodes in blue,

**Table 2** Setup of the mechanical simulations

Basic material	Aluminum (7075-T6) [30]
Basic material Young modulus	72 GPa
Basic material Poisson ratio	0.3
Total applied stress	5.4 MPa
Foam surface model BB* length (*x*-axis) (Fig. 17)	380.66 µm ≈ 5 cells
Foam surface model BB width (*y*-axis) (Fig. 17)	379.30 µm ≈ 5 cells
Foam surface model BB height (*z*-axis) (Fig. 17)	100.24 µm ≈ 1 cell
Height H_L of the region where nodes are loaded (Fig. 17b)	15.0 µm (15% of foam height)
Height H_D of the region where nodal displacements are constrained (Fig. 17b)	15.0 µm (15% of foam height)

∗ BB: Bounding Box

Fig. 17 **a** Setup of the tension case study; constrained and loaded nodes in the **b** Truss and **c** reference models

Fig. 18 **a** Setup of the shear case study; constrained and loaded nodes in the **b** Truss and **c** reference models
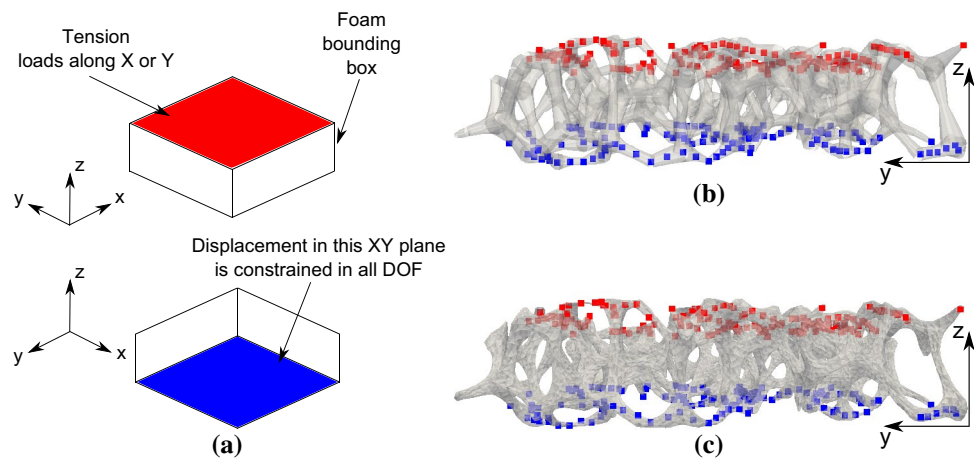
all translations are set to zero. Shear loads in *Z* direction are applied on the nodes (in red color) on the upper *X–Y* plane of the foam BB.

Shear case study The setup of this case study is shown in Fig. 18. All translations are set to zero for the nodes (in blue color) on the lower *X–Y* plane of the foam BB. Shear loads are applied on the nodes (in red color) on the upper *X–Y* plane of the foam BB. In this case, two load configurations are tested: **a** forces along *X* direction and **b** forces along *Y* direction.

4 Results and discussion

4.1 Truss model generation

The foam simplification method presented here is applied to a surface mesh of aluminum open-cell foam (see dimensions in Table 3) obtained from a CT scan (as in [21]). The input foam model presents typical manufacturing imperfections [3, 31, 32], such as

1. Curved ligaments
2. Missing cell ligaments
3. Missing cells
4. Irregular cell shape
5. Closed windows (filled cell faces)
6. Small windows (small holes in cell faces)

These manufacturing defects are retained very well in the truss model of the aluminum foam. Figure 19 shows the preservation of small holes in cell faces and filled cell faces of the aluminum foam surface model in the truss model. Figure 20 shows the complete aluminium surface model and the resulting truss model.

4.2 Truss model quality

The quality of the approximation of the Truss model with respect to the original Full B-Rep model is measured in terms of the porosity preservation and Hausdorff distances.

Fig. 19 Preservation by truss model (**b**) of local geometry and topology of foam (**a**). Full B-Rep: GREY, Truss: GREEN

Small window

Closed window

(a)

(b)
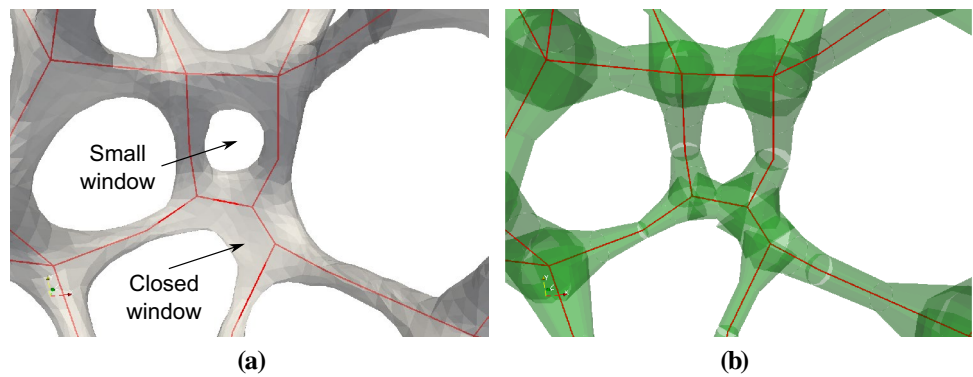
Fig. 20 Geometry simplification of the foam model. **a** Full B-Rep. **b** Truss abstraction of (**a**). Full B-Rep: GREY, Truss: GREEN

(a)

(b)
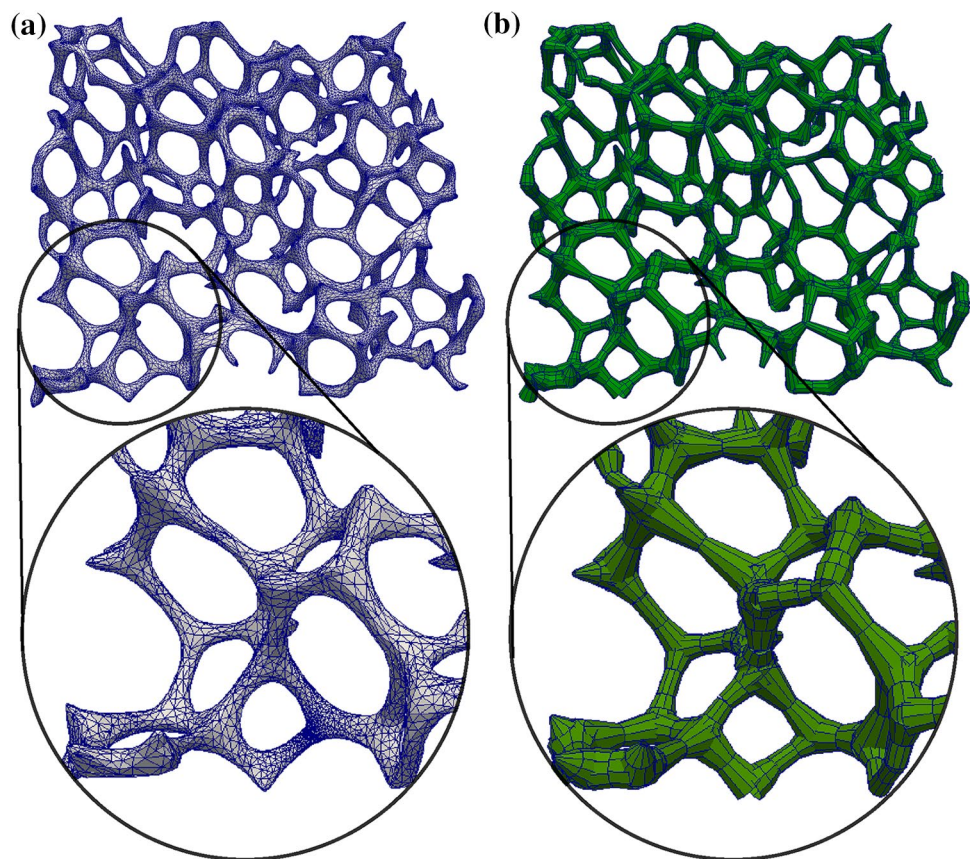
4.2.1 Porosity preservation

As proposed in [3, 4], the porosity of the full B-Rep and truss models is compared to quantify how well the truss model approximates the geometry of the full B-Rep one. The porosity ϕ is defined as $\phi = (Vol_{BB} - Vol_S)/(Vol_{BB})$, where Vol_{BB} and Vol_S are the BB and solid phase volumes of the foam model, respectively. The result of the porosity computation is presented in Table 3 for the studied domain.

4.2.2 Hausdorff distance

The Hausdorff distance between the surfaces of (a) the full B-Rep model and (b) the obtained truss model from (a) is computed to quantify how well the truss model approximates the full B-Rep one. Notice that low Hausdorff distance values require the correct positioning of the truss nodes and ligaments and also an accurate estimation of their radii. Figure 21 shows the results of the normalized Hausdorff distance (H_d) computation for the test domain.
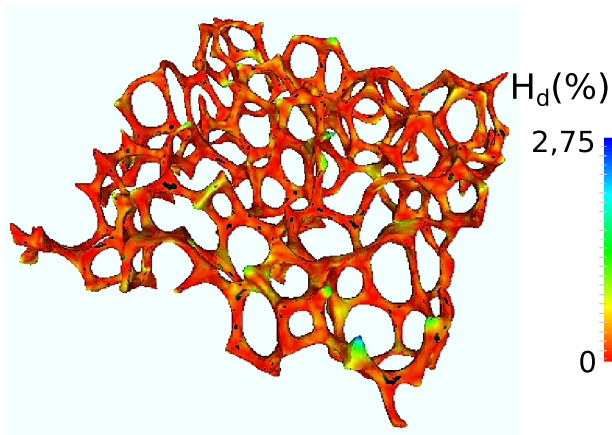
Fig. 21 Quality of the approximation in terms of the normalized Hausdorff distance H_d between the Full B-Rep and Truss models

Table 3 Summary of the setup and geometry simplification results

Domain Size (μm)	$380 \times 379 \times 100$	
D_t (μm)	2	
D_e (μm)	10	
D_n (μm)	15	
L_s (μm)	4	
Max_Iters	4	
ϕ	Surface model	0.9440
	Truss model	0.9424
	Relative error (%)	0.17
H_d	Max (%)	2.75
	Mean (%)	0.2

H_d is normalized with respect to the diagonal of the BB domain. The color of the various regions indicates the quality of the approximation in that particular neighborhood.

Table 3 presents the obtained maximum and mean values of H_d.

## 4.3 Mechanical simulations

4.3.1 Computational resources

Assuming that the number of tetrahedral and strut elements that are used in the reference and truss models, respectively, to approximate a foam ligament is constant (in average), the computational resources demanded by the models can be expressed as a function of the number of ligaments of a foam sample. This is a rough approximation but helps to gain insight into the computational complexity of the foam models at hand.

Figure 22 presents the number of elements, the number of equations, and memory demanded by the foam models vs. the number of ligaments. The mentioned computational resources are directly reported by ANSYS at the moment of executing the simulations (case studies). Figure 22 shows a large reduction (above 90%) of the computational resources demanded by the truss model with respect to the ones required by the reference model. Notice that the significant reduction in the computational resources required by the truss model enables the simulation of large foam domains that are unfeasible with the Full B-rep model (large number of 3D elements would be required) due to hardware or license constraints.

4.3.2 Tension case study

Figures 23, 24 and 25 show the nodal displacements along Z, X and Y directions, respectively, of the reference and truss models obtained for the tension case study.

The nodes selected for the estimation of the apparent Young's Modulus E_z are the ones with $c_z \geq 0.8 * Z_{max}$, where
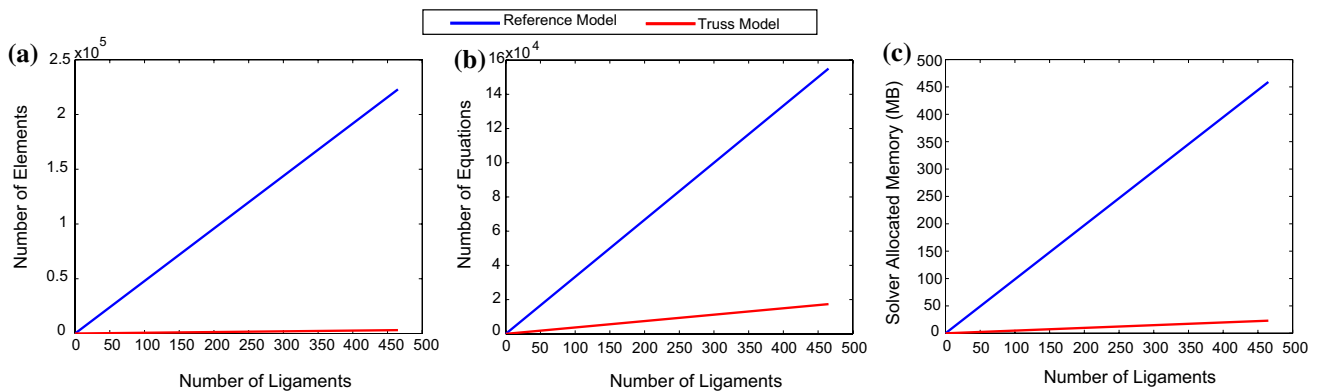
Fig. 22 Experimental expenses of resources as per commercial FE code ANSYS accounting. **a** Number of elements, **b** number of equations and **c** memory (MB) allocated by the FE solver as a function of the number of ligaments in foam domain
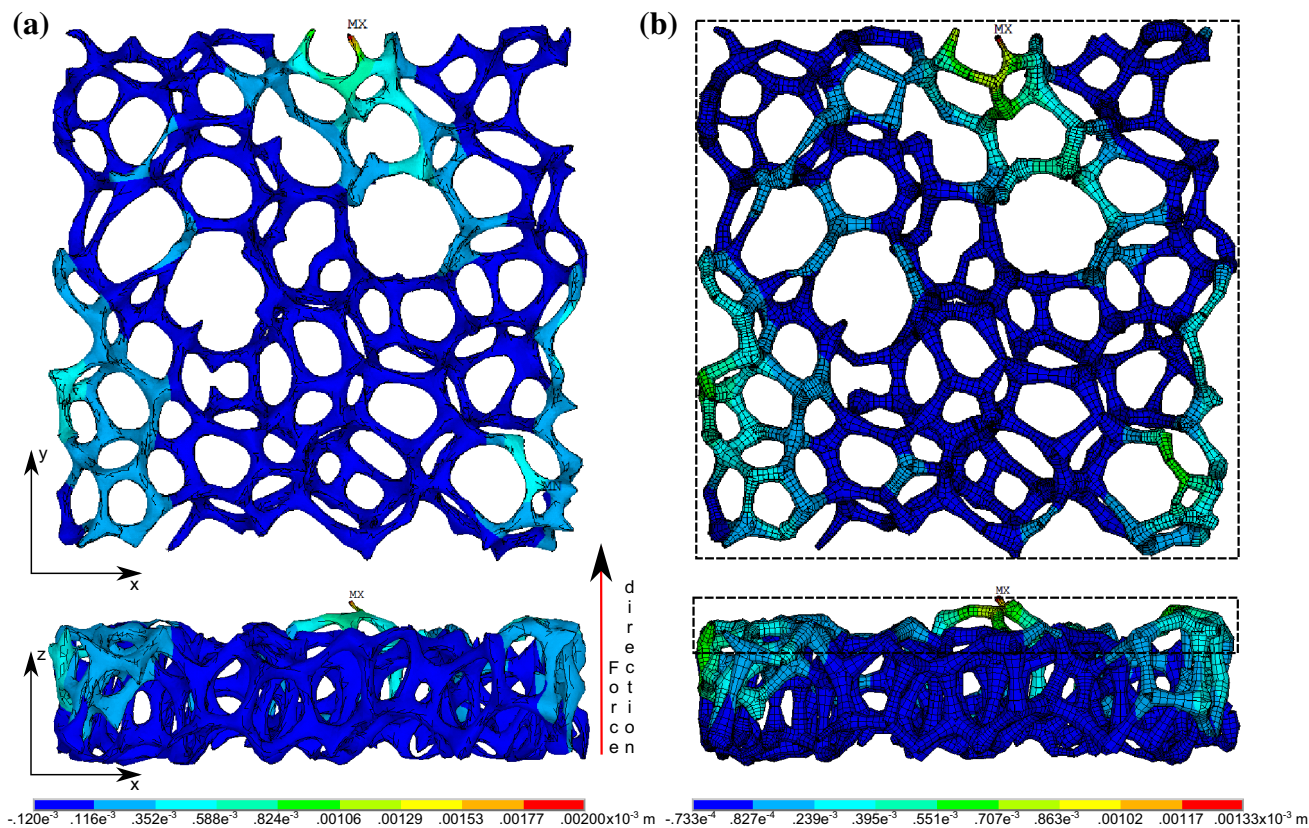
Fig. 23 Nodal displacements in Z direction of the: **a** reference and **b** Truss models. Foam deformation is not noticeable in this drawing

c_z is the node coordinate in Z and Z_{max} is the maximum coordinate in Z of all nodes of the foam models. The dashed box in Fig. 23b encloses the nodes that comply with the mentioned condition in the truss model. E_z is computed as per Eq. 1, where F is the total applied force, A_0 is the area of the X-Y plane of the foam BB, L_0 is the height of the foam BB and ΔL is the change in the height of the foam. ΔL is estimated as the average of the displacements in Z of the previously selected nodes. The results of the estimation of E_z are presented in Table 4.

$$E = \frac{\sigma}{\epsilon} = \frac{F/A_0}{\Delta L/L_0} \quad (1)$$

The apparent Poisson's Ratio is computed as per Eq. 2. In this case study, $\epsilon_i = \epsilon_z$. ϵ_j takes values of $\epsilon_j = \epsilon_x$ and $\epsilon_j = \epsilon_y$, when computing V_{zx} and V_{zy}, respectively.

$$V_{ij} = -\epsilon_j/\epsilon_i \quad (2)$$

To compute V_{zx} and V_{zy}, a selection of nodes at half height of the foam BB is performed, as indicated by the dashed

boxes in Figs. 24 and 25. To estimate ΔL in the j direction, nodes with coordinate in j (c_j) that comply with $c_j \leq j_{min} + 0.3 * L_j \vee c_i \geq j_{max} - 0.3 * L_j$ are selected. Here, j_{min} and j_{max} are the minimum and maximum coordinates of the foam BB in j direction and L_j is the length foam BB in j direction. The height of each selection box is 20% of the height of the foam BB. Finally, $\Delta L = |\Delta \bar{L}_1| + |\Delta \bar{L}_2|$, where $\Delta \bar{L}_1$ and $\Delta \bar{L}_2$ are the mean displacements of the nodes enclosed in each selection box. The results of the estimation of V_{zx} and V_{zy} are presented in Table 4.

The values of the apparent elastic properties in Table 4 are within the expected range for open-cell foams according with experimental data in [28, 31]. The estimated apparent Young's Modulus with the truss model is within 89% agreement with the reference model, and the apparent Poisson's Ratio presents a 98% agreement for the ZX component, and 99% for the ZY component between the truss and reference model. The obtained E_z of the truss model indicates that this model is less stiff than the reference one.
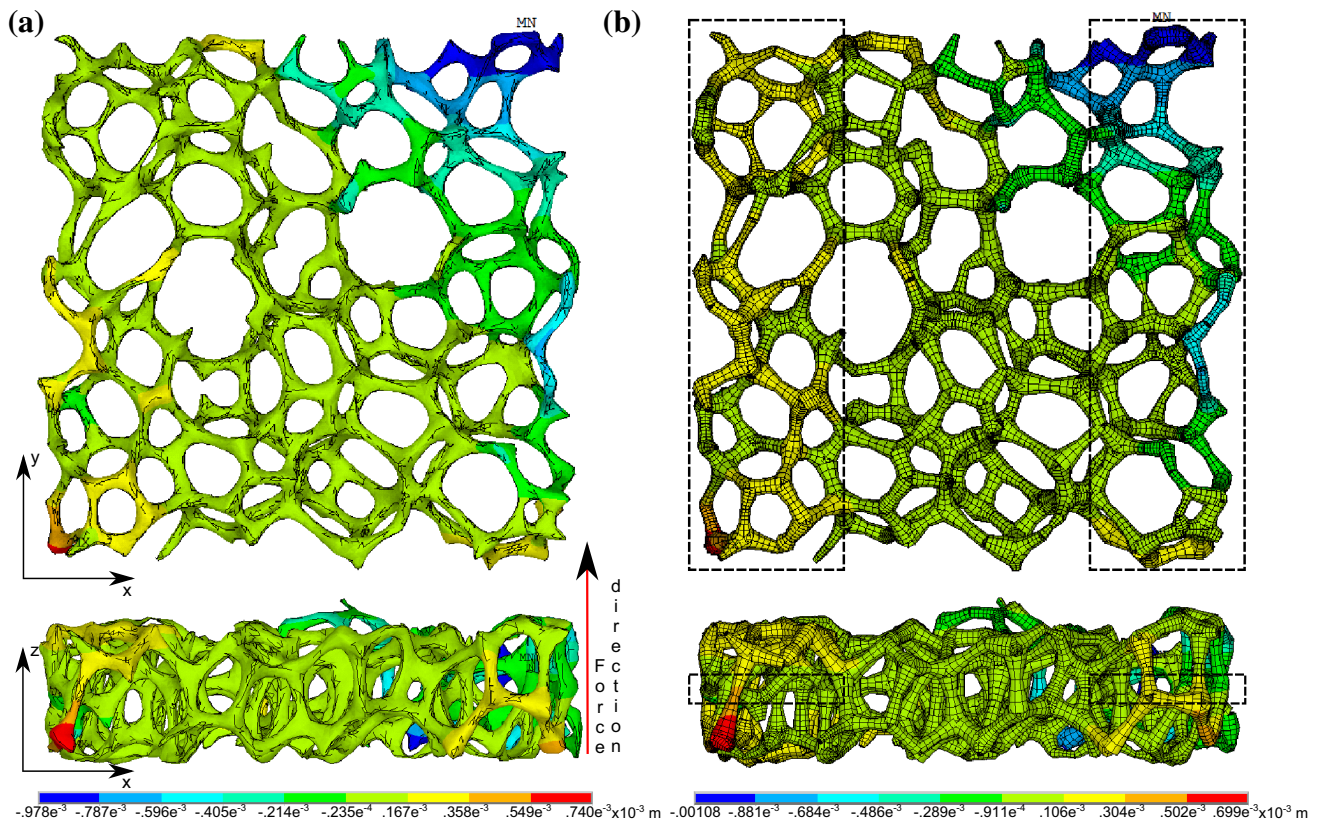
Fig. 24 Nodal displacements in X direction of the **a** reference and **b** Truss models. Foam deformation is not noticeable in this drawing

4.3.3 Shear case study

Figures 26 and 27 show the nodal displacements along X and Y directions, respectively, of the reference and truss models obtained for the two tested loading setups (shear stresses in the X and Y directions). The nodal displacements obtained for both models present similar magnitudes and distributions for all load cases.

The nodes selected for the estimation of the shear moduli G_x and G_y are the ones with $c_z \geq 0.8 * Z_{max}$, where c_z is the node coordinate in Z and Z_{max} is the maximum coordinate in Z of the foam BB. The selection boxes enclosing the nodes that comply with the mentioned condition are shown in Figs. 26b and 27b for the truss model.

G_x and G_y are computed as per Eq. 3, where F_i is the total applied force in i direction, A_0 is the area of the X-Y plane of the foam BB, L_0 is the height of the foam BB, and Δi is the transverse displacement in i direction. Δi is estimated as the mean displacement in i direction of the previously selected nodes. The results of the estimation of G_x and G_y are presented in Table 5.

$$G_i = \frac{F/A_0}{\Delta i/L_0} \tag{3}$$

The obtained estimations of the shear modulus in Table 5 are within the range of typical values for open-cell foams in [31]. The estimated G_x and G_y of the truss model are in 83 and 86% agreement with respect to the reference model, respectively. Furthermore, the relative error between models is within an admissible range for the comparison between different methods (i.e. [33]).

Notice that since the struts junctions are not meshed, the truss model is not suitable for FE analyses that require a full B-Rep of the foam (e.g. computational fluid dynamics).

-.489e^{-3} -.374e^{-3} -.258e^{-3} -.142e^{-3} -.264e^{-4} .893e^{-4} .205e^{-3} .321e^{-3} .437e^{-3} .552e^{-3}x10^{-3} m

-.469e^{-3} -.342e^{-3} -.215e^{-3} -.885e^{-4} .382e^{-4} .165e^{-3} .292e^{-3} .418e^{-3} .545e^{-3} .672e^{-3}x10^{-3} m
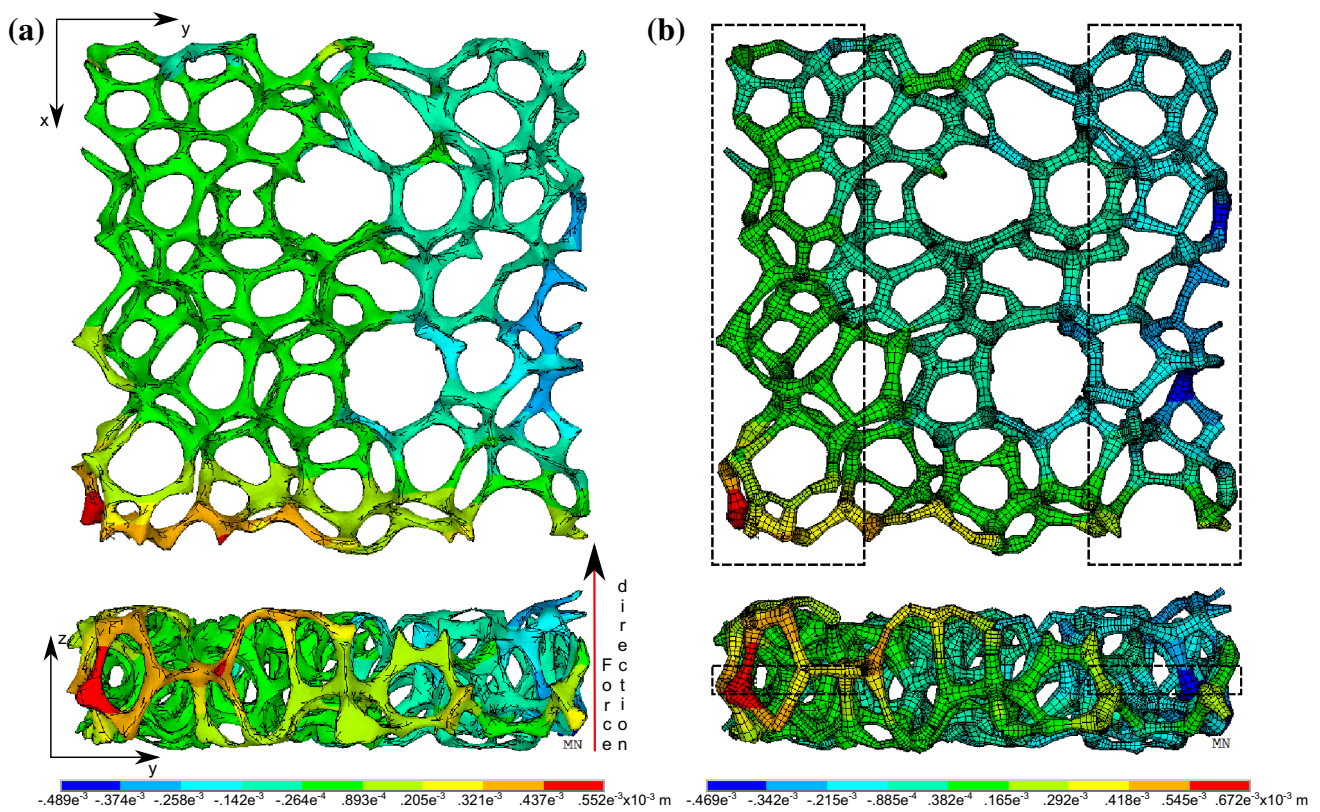
Fig. 25 Nodal displacements in Y direction of the **a** Reference and **b** Truss models. Foam deformation is not noticeable in this drawing

Table 4 Result of the estimation of apparent elastic properties in the tension case study

Apparent property	Symbol	Tetrahedral model	Truss model	Relative error (%)
Young Mod. (Pa)	E_z	2.8067e8	2.5015e8	10.87
Poisson ratio	V_{zx}	0.3456	0.3386	2.03
Poisson ratio	V_{zy}	0.3002	0.3024	0.73

5 Conclusion

This article presents a novel computational method to produce a locally accurate geometry simplification of open-cell foams. The presented algorithm addresses foams whose ligaments have cross-sections of approximately circular shape. The foam geometry is approximated with a truss model with struts being truncated cones. This approach keeps the geometry and topology of the specific material sample. In this way, the manufacturing imperfections of the foam sample (e.g. missing ligaments and cells, cell shape irregularity, filled cell faces, etc.) are retained in the truss model. This local accurate simplification of specific material samples is absent in previous works.

The geometrical accuracy of the truss model is assessed in terms of porosity (a popular parameter for porous material characterization) and Hausdorff distance. The porosity and Hausdorff distance results show that the
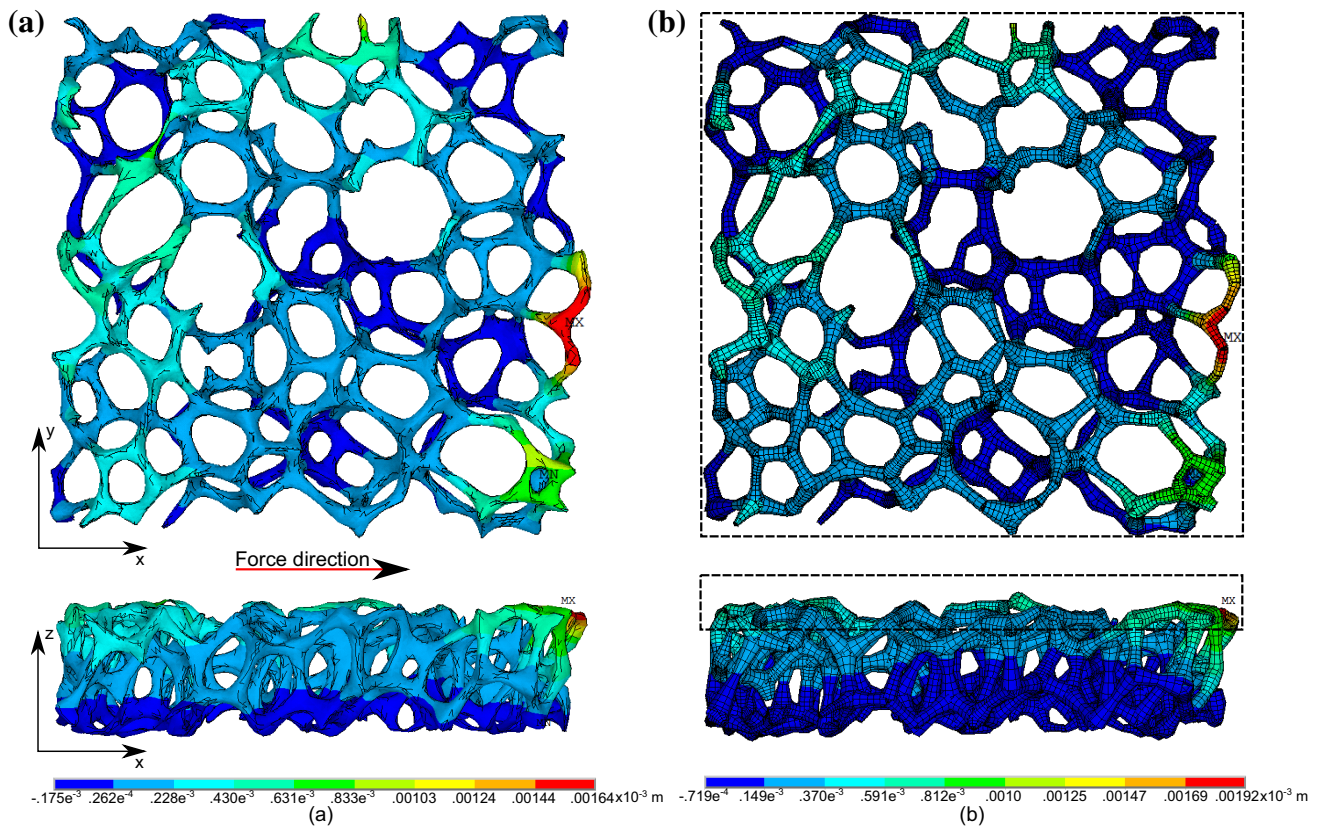
Fig. 26 Transverse nodal displacements in *X* of the **a** reference and **b** Truss models. Foam deformation is not noticeable in this drawing

truss model closely approximates the full B-Rep model of the foam.

The performance of the truss model for mechanical simulations is assessed in tension and shear case studies. The estimations of the elastic properties (apparent Young's modulus, Poisson's ratio and shear modulus) of the truss model approximate with a maximum error of 16% the ones of a reference model (tetrahedral mesh of the Full B-Rep model). Furthermore, the computational resources (i.e. number of elements and equations, memory required by the FEM solver) demanded by the truss model for FE analyses are less than 10% of the ones required for the reference model. The truss model enables to simulate domains that are unfeasible with a Full B-rep model due to hardware or license constraints.

The obtained results show the feasibility of the implemented method to produce a simplified geometric model for open-cell porous materials and that the produced model can be used for efficient FEA simulation. Such results encourage to proceed with an extensive validation and extension of the method.

6 Future research opportunities

The methodology presented in this manuscript entails the following future work for interested researchers: (a) assessment of the truss model performance for heat transfer analysis, (b) adaptation of the truss model for computational fluid dynamics analysis, (c) adaptation of the truss model generation method to approximate ligaments with non-circular cross-section, (d) assessment of the performance of the truss model in non-linear mechanics setups, (e) development of alternative approaches to estimate elastic properties (torsion, elongation, etc.) to accommodate the Testing Material Standards, and (f) heuristics for automatic parameter tuning of the simplification method.
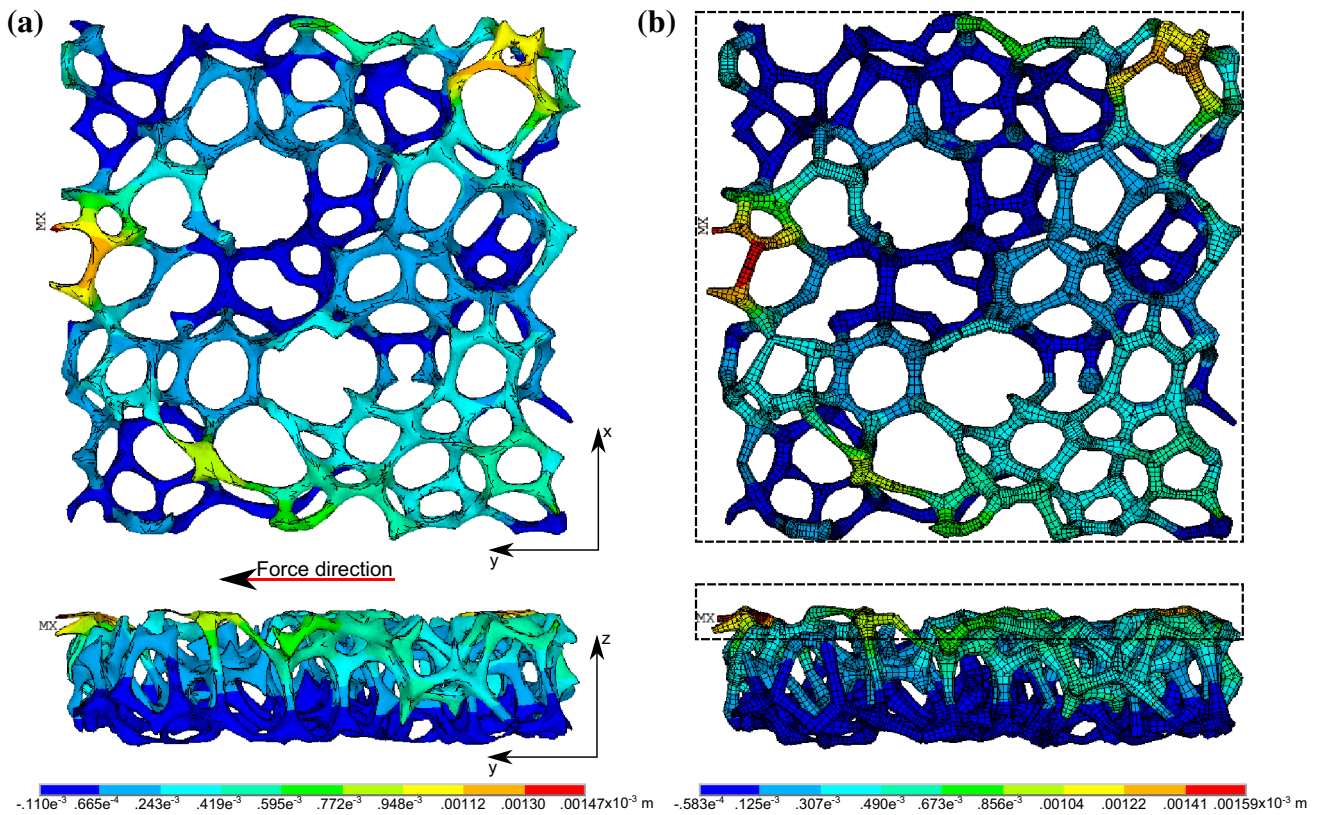
Fig. 27 Transverse nodal in *Y* of the **a** reference and **b** Truss models. Foam deformation is not noticeable in this drawing

Table 5 Result of the estimation of apparent elastic properties in the shear case study

Apparent property	Symbol	Tetrahedral model	Truss model	Relative error (%)
Shear mod. (Pa)	G_x	1.2397e8	1.0396e8	16.14
Shear mod. (Pa)	G_y	1.1140e8	0.95721e8	14.07

References

1. Kou XY, Tan ST (2010) A simple and effective geometric representation for irregular porous structure modeling. Comput Aided Des 42(10):930–941
2. Li H, Yang J, Su P, Wang W (2012) Computer aided modeling and pore distribution of bionic porous bone structure. J Central South Univ 19:3492–3499
3. Ettrich J, August A, Roelle M, Nestler B (2014) Digital representation of complex cellular structures for numerical simulations. In Cellular Materials: Proceedings CELLMAT 2014, pp 1–8. Deutsche Gesellschaft fuer Materialkunde,Fraunhofer-Institut fuer Angewandte Materialforschung
4. De Jaeger P, TJoen C, Huisseune H, Ameel B, De Paepe M (2011) An experimentally validated and parameterized periodic unit-cell reconstruction of open-cell foams. J Appl Phys 109(10):103519
5. Lautensack C (2008) Fitting three-dimensional laguerre tessellations to foam structures. J Appl Stat 35(9):985–995
6. Jang W, Kraynik AM, Kyriakides S (2008) On the microstructure of open-cell foams and its effect on elastic properties. Int J Solids Struct 45(7):1845–1875
7. Redenbach C (2009) Microstructure models for cellular materials. Computat Mater Sci 44(4):1397–1407
8. Jang W, Hsieh W, Miao C, Yen Y (2015) Microstructure and mechanical properties of alporas closed-cell aluminium foam. Mater Char 107:228–238
9. Michailidis N, Stergioudi F, Omar H, Tsipas DN (2010) An image-based reconstruction of the 3d geometry of an al open-cell foam and fem modeling of the material response. Mech Mater 42(2):142–147
10. Saenger EH, Uribe D, Jänicke R, Ruiz O, Steeb H (2012) Digital material laboratory: wave propagation effects in open-cell aluminium foams. Int J Eng Sci 58:115–123
11. Natesaiyer K, Chan C, Sinha-Ray S, Song D, Lin CL, Miller JD, Garboczi EJ, Forster AM (2015) X-ray ct imaging and finite element computations of the elastic properties of a rigid organic foam compared to experimental measurements: insights into foam variability. J Mater Sci 50(11):4012–4024
12. Ranut P, Nobile E, Mancini L (2014) High resolution x-ray microtomography-based cfd simulation for the characterization of flow permeability and effective thermal conductivity of aluminum metal foams. Experimental Thermal and Fluid Science
13. Zafari M, Panjepour M, Emami MD, Meratian M (2015) Microtomography-based numerical simulation of fluid flow and heat transfer in open cell metal foams. Appl Thermal Eng 80:347–354

14. Lu Z, Liu Q, Chen X (2014) Analysis and simulation for tensile behavior of anisotropic open-cell elastic foams. Appl Math Mech 35:1437–1446

15. Boomsma K, Poulikakos D (2001) On the effective thermal conductivity of a three-dimensionally structured fluid-saturated metal foam. Int J Heat Mass Transf 44(4):827–836

16. Jang W, Kyriakides S, Kraynik AM (2010) On the compressive strength of open-cell metal foams with kelvin and random cell structures. Int J Solids Struct 47(21):2872–2883

17. Randrianalisoa J, Baillis D, Martin CL, Dendievel R (2015) Microstructure effects on thermal conductivity of open-cell foams generated from the laguerre-voronoï tessellation method. Int J Thermal Sci 98:277–286

18. Kanaun S, Tkachenko O (2006) Mechanical properties of open cell foams: Simulations by laguerre tesselation procedure. Int J Fracture 140(1–4):305–312

19. Liebscher A, Proppe C, Redenbach C, Schwarzer D (2012) Uncertainty quantification for metal foam structures by means of image analysis. Probabilistic Eng Mech 28:143–151

20. Lorensen William E, Cline Harvey E (1987) Marching cubes: a high resolution 3D surface construction algorithm. SIGGRAPH Comput Graph 21(4):163–169

21. Uribe D, Osorno MC, Steeb H, Saenger EH, Ruiz O (2014) Geometric and numerical modeling for porous media wave propagation. In: I. Horváth and Z. Rusák, editors, Proceedings of Tools and Methods of Competitive Engineering TMCE 2014, pages 685–694, Budapest, Hungary, May 19–23. ISBN 978-94-6186-176-4

22. Tagliasacchi A, Alhashim I, Olson M, Zhang H (2012) Mean curvature skeletons. Comput Graphics Forum 31(5):1735–1744

23. Livesu M, Scateni R (2013) Extracting curve-skeletons from digital shapes using occluding contours. Visual Comput 29(9):907–916

24. Usai F, Livesu M, Puppo E, Tarini M, Scateni R (2015) Extraction of the quad layout of a triangle mesh guided by its curve skeleton. ACM Trans Graphics (TOG) 35(1):6

25. Mean curvature skeletons. https://github.com/ataiya/starlab-mcfskel. Accessed: 2016-10-18

26. Livesu M, Muntoni A, Puppo E, Scateni R (2016) Skeleton-driven adaptive hexahedral meshing of tubular shapes. Comput Graphics Forum 35(7):237–246

27. Andrews E, Sanders W, Gibson Lorna J (1999) Compressive and tensile behaviour of aluminum foams. Mater Sci Eng: A 270(2):113–124

28. Nieh TG, Higashi K, Wadsworth J (2000) Effect of cell morphology on the compressive properties of open-cell aluminum foams. Mater Sci Eng: A 283(1):105–110

29. Patrick JV (2016) Investigation of the behavior of open cell aluminum foam. Master's thesis, University of Massachusetts-Amherst

30. Giner E, Sabsabi M, Ródenas JJ, Fuenmayor FJ (2014) Direction of crack propagation in a complete contact fretting-fatigue problem. Int J Fatigue 58:172–180

31. Ashby MF, Evans T, Fleck NA, Hutchinson JW, Wadley HNG, Gibson LJ (2000) Metal foams: a design guide: a design guide. Elsevier,

32. Lu Z, Liu Q, Huang J (2011) Analysis of defects on the compressive behaviors of open-cell metal foams through models using the fem. Mater Sci Eng: A 530:285–296

33. Andrä H, Combaret N, Dvorkin J, Glatt E, Han J, Kabel M, Keehm Y, Krzikalla F, Lee M, Madonna C et al (2013) Digital rock physics benchmarks Part II: computing effective properties. Comput Geosci 50:33–43